ACS Catalysis

LETTER

pubs.acs.org/acscatalysis

Predictive Structure−Reactivity Models for Rapid Screening of Pt-Based Multimetallic Electrocatalysts for the Oxygen Reduction Reaction

Hongliang Xin, Adam Holewinski, and Suljo Linic*

Department of Chemical Engineering, University of Michigan, Ann Arbor, Michigan 48109-2136, United States

Supporting Information

ABSTRACT: Due to the immense phase space of potential alloy catalysts, any rigorous screening for optimal alloys requires simple and accurate predictive structure−reactivity relationships. Herein, we have developed a model that allows us to accurately predict variations in adsorption energy on alloy surfaces based on easily accessible physical characteristics of the metal elements that form the alloy—mainly their electronegativity, atomic radius, and the spatial extent of valence orbitals. We have developed a scheme relating the geometric structure and local chemical environment of active Pt sites to the local chemical reactivity of the sites in the electrochemical oxygen reduction reaction (ORR). The accuracy of the model was verified with density functional theory (DFT) calculations. The model allows us to screen through large libraries of Pt alloys and identify many potentially promising ORR alloy catalysts. Some of these materials have previously been tested experimentally and shown improved performance compared to pure Pt. Since the model is grounded on validated theories of chemisorption on metal surfaces, it can be used to identify the critical physical features that characterize an optimal alloy electrocatalyst for ORR and propose how these features can be engineered.

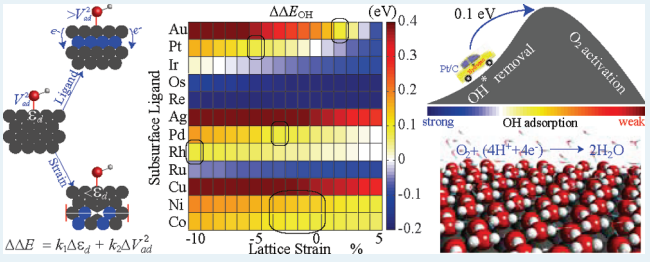

KEYWORDS: density functional calculations, fuel cells, platinum, rapid screening, alloys, oxygen reduction reaction

The primary cause of efficiency loss in low temperature proton exchange membrane (PEM) fuel cells is the sluggish kinetics of the oxygen reduction reaction (ORR), $4(H^+ + e^-) + O_2 \rightarrow 2H_2O$, at the cathode.[1−3] Though Pt is the best pure-metal ORR electrocatalyst, it still exhibits an appreciable overpotential because of the strong binding of surface hydroxyl (OH) to surface Pt sites, which poisons Pt at high operating potentials.[1,4,5] The key objective in formulating optimal Pt alloys for ORR is to identify elements that would, when alloyed with Pt, electronically perturb the surface Pt sites so that they bind OH with slightly lower adsorption energy (∼0.1 eV less exothermic) than pure Pt.[3,5,6] In this Letter, we propose a model that accomplishes this objective, allowing us to rapidly screen through the immense phase space of Pt alloys. In our analysis, we focus on Pt skin alloys, characterized by a surface occupied completely by Pt atoms. This model system is consistent with experimental and computational findings showing that under relevant electrochemical conditions the surface of Pt alloys is occupied by Pt atoms.[7−11] We note that the model is very general, and it is not limited to the Pt-skin alloy structures, i.e., it could be applied to nonhomogeneous surfaces.

We have previously shown that the change in the OH adsorption energy on a Pt site as a function of the local chemical environment of the site can be described by focusing on the interactions of the local *d*-states of the site with the OH adsorbate states.[12] More specifically, we showed that the change in the OH adsorption energy ($\Delta\Delta E$), in response to the change in the local chemical environment of the Pt surface site, is governed by two physical characteristics of the site: the average energy of electronic d-states projected on the adsorption Pt site (i.e., the center of d-band, ε_d), and the interatomic matrix element (V_{ad}^2)[13] describing the coupling strength of OH valence states with the substrate d-band. For small perturbations in the local chemical environment of the Pt site, for example induced by alloying, the change of adsorption energy ($\Delta\Delta E$) can be written as a linear function of $\Delta\varepsilon_d$ and ΔV_{ad}^2 as shown in eq 1 ($k_1 \approx -0.20$, $k_2 \approx 1.95$ eV^{-1}, see the Supporting Information for details).

$$\Delta\Delta E = k_1\Delta\varepsilon_d + k_2\Delta {V_{ad}}^2 \quad (1)$$

On a conceptual level, the first term in eq 1 describes the covalent attraction due to the hybridization between an adsorbate state (orbital) and substrate d-states, while the second term describes the Pauli repulsion due to the energy cost associated with the orbital orthogonalization as illustrated in Figure 1.[14,15] We have previously demonstrated that when $\Delta\varepsilon_d$ and $\Delta {V_{ad}}^2$ are calculated using self-consistent density functional theory (DFT),[12,16] the model gives excellent agreement with the DFT-calculated OH adsorption energies on Pt-based alloys.[12]

Received: September 9, 2011
Revised: November 1, 2011
Published: November 16, 2011

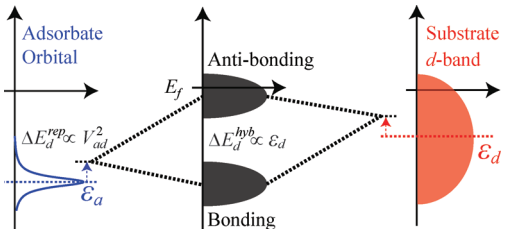

Figure 1. Schematic illustration of the chemical bonding between adsorbate states and metal d-states, which leads to an upward shift in energies due to the Pauli repulsion, followed by the formation of bonding and antibonding states because of the orbital hybridization.

We now make eq 1 useful for rapid screening of optimal ORR alloy catalysts by developing simple expressions, which do not require computationally expensive quantum-chemical calculations, to evaluate the change in the d-band center ($\Delta\varepsilon_d$) of the Pt adsorption site and the change in OH−Pt coupling matrix element, in response to the perturbation of the local chemical environment of Pt due to alloying. The accuracy of the model was verified with fully optimized self-consistent DFT calculations within the generalized gradient approximation (GGA-PW91) using ultrasoft pseudopotentials[17] as implemented in DACAPO. The details of calculation parameters have been provided in previous studies[12,16] and the Supporting Information.

It has been shown based on Muffin-Tin-Orbital (MTO) theory within the tight binding approximation that, for an adsorbate on a metal site, the coupling matrix element, V_{ad}, is a function of the adsorbate-metal bond distance, d, and the spatial extent of the metal d-orbital (r_d) ($V_{ad} \propto r_d^{3/2}/d^{7/2}$).[13] For OH adsorption on Pt sites, r_d is identical, irrespective of the chemical environment of the site (i.e., it is an inherent property of the Pt atom). Therefore the change in OH−Pt coupling matrix, ΔV_{ad}^2, in response to the formation of an alloy (more specifically the change of the local chemical environment) is only a function of the change in the metal−OH bond distance. To determine the relative OH−Pt bond distance for different Pt alloys, we have employed extensive DFT studies which established that, on geometrically similar Pt sites of alloys, the bond distance is linearly correlated with the difference in the geometric mean of the Mulliken electronegativity of the local Pt atom and its neighboring atoms, as shown in eq 2. The proportionality coefficient, $\gamma = -0.094$, was obtained by linearly fitting the metal−OH bond distance calculated using DFT for a subset of Pt alloy surfaces. Comparison of bond distances predicted by the model to DFT calculations shows good agreement (RMSE ≈ 0.01 Å) for many different families of Pt alloys as shown in Figure 2.

$$\Delta d = \gamma([\prod_i^N \chi_i^{nn}]^{1/N} - \chi_{Pt}) = \gamma\Delta\chi \qquad (2)$$

The observed relationship between the change in electronegativity and the metal−OH bond distance can be rationalized by the fact that the main fraction of OH adsorption energy on Pt sites comes from the interaction of the OH valence states with the free-electron-like sp-band of the substrate. Thus, the interaction between the sp-band and the OH states, to a large degree, governs the metal−OH bond distance.[5] Because of the difference in the electronegativity of Pt and the neighboring atoms in an alloy, there is a transfer of electron density, changing the filling

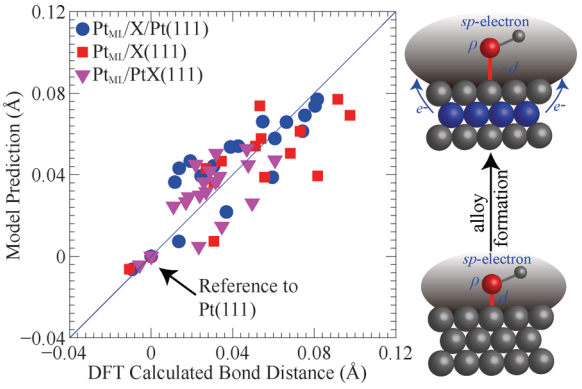

Figure 2. DFT calculated metal−OH bond distance on various Pt alloy surfaces correlated with the prediction of the model in eq 2. The sketch is an illustration of the effect of the change in the surface electron density on the adsorbate−substrate bond distance.

of the sp-band of Pt (i.e., the free-electron density is perturbed). This change in the local electron density affects the adsorbate−substrate bond length at the local site as illustrated in Figure 2.[18] The process can be understood in terms of the adsorbate seeking the regions of optimal electron density on a metal surface. The electron density around local adsorption sites changes in response to the formation of an alloy, and the adsorbate responds by changing the bond distance and finding a new geometry with optimal electron density. In practice, this means that if a Pt surface site is surrounded by less electronegative atoms, charge will be transferred to the Pt site, and the OH adsorbate will move further away, lengthening the bond. We show in the Supporting Information that the same relationship exists for many other adsorbates on Pt alloy surfaces.

As shown in eq 1, the other major quantity governing the relative OH adsorption energy on Pt sites is the center of the electronic d-band (ε_d) projected on the site. It has been shown previously that for many alloys, the shift in the center of the d-band ($\Delta\varepsilon_d$) projected on individual atoms, induced by the change in the local chemical environment of the site, is uniquely determined by the change in the d-band width (the spread of d-states) as shown in eq 3 and described in more detail below.[16,19,20]

$$\Delta W_d^i \propto \Delta\varepsilon_d^i = \alpha\Delta \sum_j V_{dd}^{ij} + \beta\Delta\chi \qquad (3)$$

The change in the d-band width for a given substrate atom is governed by the interaction of the d-orbitals of that atom with the valence orbitals of neighboring substrate atoms (both d-states and the delocalized sp-states).[13] The interaction with neighboring d-orbitals is captured by the d−d interatomic matrix element (V_{dd}) describing the d-coupling strength.[13,21−23] This is a function of the bond distance between neighboring atoms and the spatial extent of the d-orbitals: $V_{dd}^{ij} \propto r_{d_i}^{3/2} r_{d_j}^{3/2}/d_{ij}^5$.[13,16,21,22,24] The spatial extent of d-orbital (r_d) is an intrinsic property of the pure metal atom.[13] In our analysis, we used r_d values calculated using MTO theory within the tight binding approximation.[13] The parameter d_{ij} is the distance between metal atoms i and j in the substrate. Finally, the change in the d-band width because of interaction with the free-electron-like sp-band can be described in terms of the difference in electronegativity (governing sp-electron density), $\Delta\chi$ (defined in eq 2).[13,25] The parameters $\alpha = -6.21$ in eq 3 was obtained by linearly fitting

dx.doi.org/10.1021/cs200462f |ACS Catal. 2012, 2, 12−16

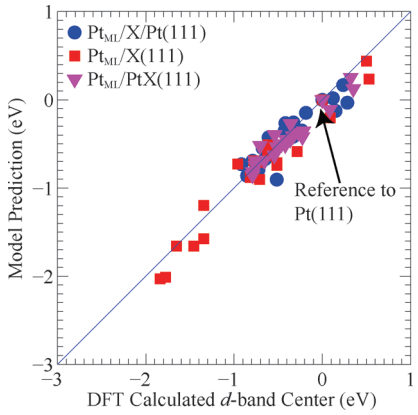

Figure 3. DFT calculated local d-band center of various Pt alloy surfaces correlated with the model prediction using eq 3.

DFT-calculated d-band centers for strained surfaces of pure Pt, while β = 0.55 eV was obtained based on the analysis of a subset of Pt alloy substrates (in this subset d_{ij} was obtained using geometry optimization within the DFT framework, for further details please consult Supporting Information).[21,22] Figure 3 shows a parity plot comparing the model-predicted d-band center via eq 3 to the DFT-calculated *d*-band center for different families of Pt alloys. DFT-optimized bond distances between neighboring atoms (d_{ij}) were used to obtain V_{ij} in this comparison. Figure 3 shows that if the DFT-calculated bond distances (d_{ij}) are used, the model predicts the change of *d*-band center very well with RMSE≈0.1 eV. For screening through a large space of alloys, the bond distance (d_{ij}) can be obtained with reasonable accuracy from generalization of Vegard's law as described in the Supporting Information and implemented in Figure 4.

The practical value of eqs 1−3 is that the relative adsorption energy of OH (with respect to pure Pt) and therefore the relative ORR activity of Pt sites on various Pt alloys can be calculated using only physical characteristics of the constituent metal elements—mainly their electronegativity (χ_i), spatial extent of the d-orbitals (r_d), and their atomic radii which to a large degree govern the distance between substrate atoms (d_{ij}). The proposed models allow for a rapid screening through a large phase space of Pt alloy compositions and geometries to identify those with desired catalytic properties (in this case binding OH with ∼0.1 eV lower adsorption energy than pure Pt[3,5,6]).

To illustrate the value of the model in eqs 1−3, we first use it to investigate the effect of a simultaneous change in the substrate lattice constant and the nature of subsurface metal on the OH adsorption energy on Pt surface sites. Here, the model system is a pure Pt slab, with variable lattice constant. The Pt atoms in the second layer are substituted by another element. Figure 4 shows that compression of the Pt−Pt bond in the surface layer lowers the OH adsorption energy. In this case, the compressed lattice yields an increased overlap among neighboring d-orbitals and therefore larger coupling matrix element, V_{dd}.[26] This results in a wider substrate d-band, lower d-band center, and therefore weaker OH-metal bond according to eq 1. Alloys exhibiting these structural features have been synthesized by depositing Pt monolayers pseudomorphically on a substrate with compressed lattice compared to Pt.[27,28] Figure 4 also shows that a similar outcome is accomplished in Pt alloys with the second layer rich in 3d metals. These intermetallic compounds (e.g., Pt_3Ni and

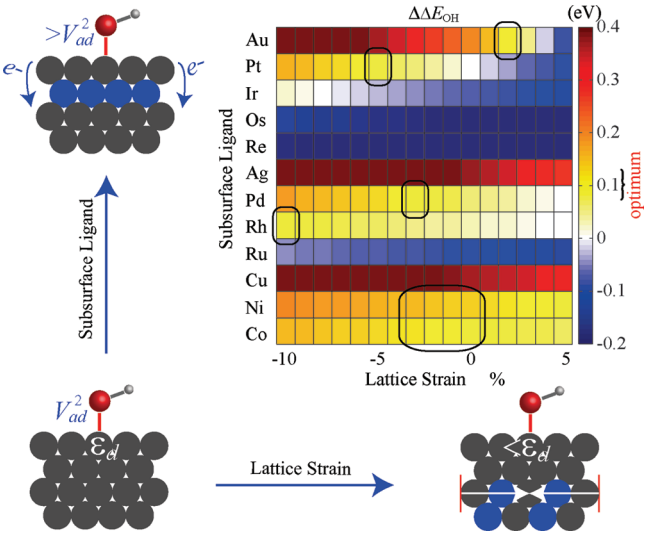

Figure 4. Model prediction of OH binding energies on Pt monolayer alloy surfaces with varying subsurface ligand (1 ML) and lattice strain (−10% to 5% expansion). Marked regions depict the alloy systems with desired catalytic properties (∼0.1 eV weaker OH binding than pure Pt). Inserts show different mechanisms by which the OH adsorption energy changes.

Pt_3Co), often called 1st generation core−shell alloys, have been identified previously experimentally, showing 2−3 times increased specific activity over pure Pt.[7,29,30] Figure 4 also shows that Pt alloys in which the Pt surface sites are coordinated with more electronegative metal atoms (e.g., Au) bind OH less strongly than pure Pt. The model in eqs 1−3 suggests that the reason for this is that the withdrawal of sp-electron density from the Pt adsorption site by Au results in a shorter OH−metal bond, which in turn increases the repulsive interaction between adsorbate states and metal d-states.[12] Similar structures have also been shown previously to exhibit enhanced ORR activity.[31,32] For example, a Pt monolayer deposited on an Au interlayer, which is supported on Au−Ni−Fe ternary alloy, has been shown to exhibit 5- to 7-fold improved specific activity compared to pure Pt.[31,32] These multilayer alloys are often referred to as 2nd generation core−shell alloys.

In general, Figure 4 gives us critical insights about the nature of the optimal Pt site for the ORR. The optimal Pt sites are characterized by a lower center of the d-band projected on the surface Pt atoms or shorter Pt−OH bond distance compared to pure Pt. In practice, there are three ways to accomplish these objectives: (1) creating alloys where surface Pt−Pt bonds are contracted, (2) coordinating Pt surface sites with 3d metals, (3) coordinating Pt surface sites with more electronegative metals (Au).

Among identified geometries, particularly appealing are the 2nd generation core−shell alloys characterized by a Pt monolayer on top of an Au−interlayer, which is then supported on an alloy core. These structures are desirable since the Au interlayer gives enhanced protection to elements in the core that are otherwise thermodynamically unstable under relevant electrochemical conditions.[31] Additionally, these materials are characterized by relatively low Pt content moderating the cost of raw materials. To further probe the 2nd generation core−shell alloys, we have applied the model in eqs 1−3 to screen through a large library of Pt monolayer alloys that belong to this family of materials. In this model, the core contained Au (75%) with two

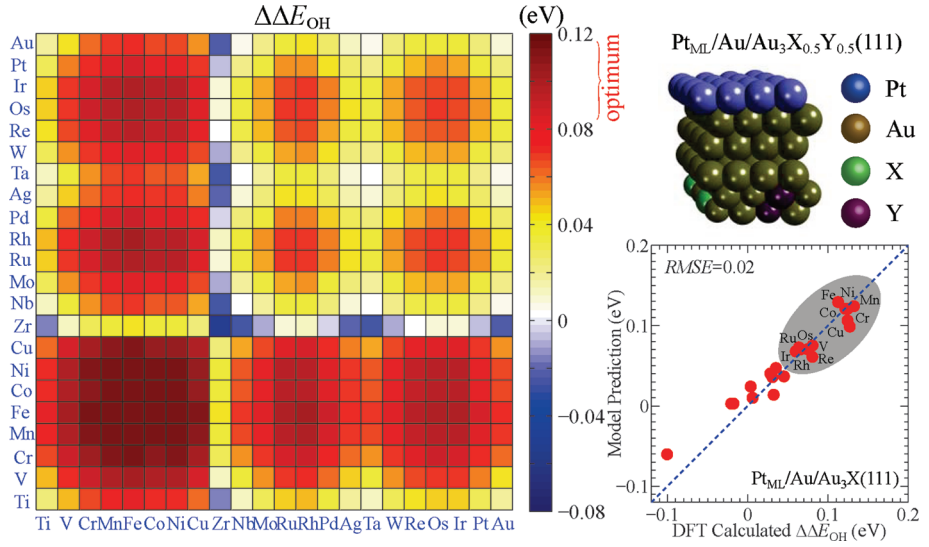

Figure 5. Model screening of OH adsorption on core−shell alloy surfaces $Pt_{ML}/Au/Au_3X_{0.5}Y_{0.5}(111)$. The parity plot in the bottom right insert shows a comparison of the OH binding energies on selected Pt monolayer alloys calculated using the model and self-consistent DFT. Top right figure shows the model system.

other (X and Y) metal elements (25% total). The lattice constant of the core structure was estimated from Vegard's law as described in the Supporting Information. The interlayer between the core and the Pt surface layer contained 3 layers of Au. The model system is established based on experimental measurements that show 3−5 layers of Au after surface annealing of Au alloy particles.[31] Essentially, surface electronic properties of these alloy materials are perturbed by the subsurface ligand of Au and the strain induced by the varying atomic radii of inner core metal elements. The model-predicted adsorption energies of OH on those alloy surfaces, relative to pure Pt, are shown in Figure 5 as a function of the X and Y elements.

Figure 5 demonstrates that the rapid screening procedure identified a large number of promising 2nd generation Pt monolayer core−shell alloys, characterized with weaker OH binding energies (∼0.1 ± 0.02 eV) than pure Pt. It is encouraging to note that some of these alloys, such as the above-mentioned $Pt_{ML}/Au/Au-Ni-Fe$, have been synthesized and tested previously, showing an improved performance compared to pure Pt.[31] Figure 5 shows that in the family of 2^{nd} generation core−shell alloys, in addition to the previously tested $Pt_{ML}/Au/Au-Ni-Fe$ alloy, there are many additional Pt alternatives. In all of these cases, a combination of Au-induced shortening in Pt−OH bond length and the change in substrate lattice constant because of alloy formation pushes the OH adsorption energy toward the desired values (∼0.1 eV lower bond strengths compared to pure Pt).

We have compared the adsorption energy calculated using the simple model in eqs 1−3 with the self-consistent DFT calculations for a few selected 2nd generation core−shell alloys ($Pt_{ML}/Au/Au_3X(111)$). These calculations showed that the model can adequately predict even small changes in the OH adsorption energy with RMSE ≈ 0.02 eV. Thorough testing of the model showed that it performs the best for alloy structures characterized by small perturbations compared to pure Pt, manifested in small alloy-induced changes in the substrate lattice constant and the Pt alloying with metals of similar electronegativity. It is important to note that alloys with these characteristics are of particular interest since they should be the easiest to synthesize.[33]

CONCLUSIONS

In summary, we have developed a physically transparent model that allows us to relate easily accessible physical characteristics of the elements that form an alloy (mainly their electronegativity, atomic radius, and the spatial extent of valence orbitals) to the catalytic performance of alloy sites. This model permits rapid screening through an enormous phase space of alloy structures and compositions using analytical expressions instead of expensive quantum-chemical calculations. We have specifically focused on Pt-based multimetallic catalysts for the electrochemical oxygen reduction reaction (ORR). We demonstrate that (1) the simple model allows for rapid screening through large libraries of Pt-alloys, (2) the model identifies almost all Pt alloys that have thus far been shown to exhibit enhanced ORR activity compared to pure Pt and suggests many new promising alloy compositions, and (3) since the model is grounded on validated theories of chemisorption on metal surfaces, it allows us to identify the critical physical features that characterize optimal alloy electrocatalyst for ORR and propose how these features can be engineered.

ASSOCIATED CONTENT

Supporting Information. Model for OH adsorption on Pt sites of alloys, details of DFT calculations, model of adsorbate bond distances to alloy surfaces, model for the prediction of d-band center of surface sites, prediction of lattice constants and surface relaxation of alloys, and tabulated data (binding energy, electronegativity, d-band center, adsorbate bond distance to the surface, etc.) for alloy structures used for obtaining model parameters. This material is available free of charge via the Internet at http://pubs.acs.org.

AUTHOR INFORMATION

Corresponding Author
*E-mail: linic@umich.edu.

■ ACKNOWLEDGMENT

We gratefully acknowledge the support of the U.S. Department of Energy DOE-BES, Division of Chemical Sciences (FG-02-05ER15686), and the National Science Foundation (CBET 1132777). S.L. also acknowledges the DuPont Young Professor grant by DuPont Corporation and the Camille Dreyfus Teacher−Scholar Award from the Camille & Henry Dreyfus Foundation.

■ REFERENCES

(1) Wang, J. X.; Marković, N. M.; Adzic, R. R. *J. Phys. Chem. B* **2004**, *108*, 4127–4133.
(2) Marković, N. M.; Schmidt, T. J.; Stamenković, V.; Ross, P. N. *Fuel Cells* **2001**, *1*, 105–116.
(3) Nørskov, J. K.; Rossmeisl, J.; Logadottir, A.; Lindqvist, L.; Kitchin, J. R.; Bligaard, T.; Jonsson, H. *J. Phys. Chem. B* **2004**, *108*, 17886–17892.
(4) Bondarenko, A. S.; Stephens, I. E. L.; Hansen, H. A.; Pérez-Alonso, F. J.; Tripkovic, V.; Johansson, T. P.; Rossmeisl, J.; Nørskov, J. K.; Chorkendorff, I. *Langmuir* **2011**, *27*, 2058–2066.
(5) Abild-Pedersen, F.; Greeley, J.; Studt, F.; Rossmeisl, J.; Munter, T. R.; Moses, P. G.; Skulason, E.; Bligaard, T.; Nørskov, J. K. *Phys. Rev. Lett.* **2007**, *99*, 016105–4.
(6) Stephens, I. E. L.; Bondarenko, A. S.; Pérez-Alonso, F. J.; Calle-Vallejo, F.; Bech, L.; Johansson, T. P.; Jepsen, A. K.; Frydendal, R.; Knudsen, B. P.; Rossmeisl, J.; Chorkendorff, I. *J. Am. Chem. Soc.* **2011**, *133*, 5485–5491.
(7) Stamenković, V. R.; Fowler, B.; Mun, B. S.; Wang, G.; Ross, P. N.; Lucas, C. A.; Marković, N. M. *Science* **2007**, *315*, 493–497.
(8) Ruban, A. V.; Skriver, H. L.; Nørskov, J. K. *Phys. Rev. B* **1999**, *59*, 15990.
(9) Adzic, R. R.; Zhang, J.; Sasaki, K.; Vukmirovic, M. B.; Shao, M.; Wang, J. X.; Nilekar, A. U.; Mavrikakis, M.; Valerio, J. A.; Uribe, F. *Top. Catal.* **2007**, *46*, 249–262.
(10) Greeley, J.; Jaramillo, T. F.; Bonde, J.; Chorkendorff, I.; Nørskov, J. K. *Nat. Mater.* **2006**, *5*, 909–913.
(11) Koh, S.; Strasser, P. *J. Am. Chem. Soc.* **2007**, *129*, 12624–12625.
(12) Xin, H.; Linic, S. *J. Chem. Phys.* **2010**, *132*, 221101–221101−4.
(13) Harrison, W. A. *Electronic Structure and the Properties of Solids: The Physics of the Chemical Bond*; Dover Publications, 1989.
(14) Hammer, B.; Nørskov, J. K. *Surf. Sci.* **1995**, *343*, 211–220.
(15) Hammer, B.; Nørskov, J. K. *Nature* **1995**, *376*, 238–240.
(16) Xin, H.; Schweitzer, N.; Nikolla, E.; Linic, S. *J. Chem. Phys.* **2010**, *132*, 111101–111101-4.
(17) Vanderbilt, D. *Phys. Rev. B* **1990**, *41*, 7892.
(18) Lambert, R. M.; Pacchioni, G. *Chemisorption and Reactivity on Supported Clusters and Thin Films*; Springer, 1997.
(19) Nikolla, E.; Schwank, J.; Linic, S. *J. Am. Chem. Soc.* **2009**, *131*, 2747–2754.
(20) Schweitzer, N.; Xin, H.; Nikolla, E.; Miller, J. T.; Linic, S. *Top. Catal.* **2010**, *53*, 348–356.
(21) İnoğlu, N.; Kitchin, J. R. *Mol. Simul.* **2010**, *36*, 633.
(22) İnoğlu, N.; Kitchin, J. R. *Phys. Rev. B* **2010**, *82*, 045414.
(23) İnoğlu, N.; Kitchin, J. R. *ACS Catalysis* **2011**, *1*, 399–407.
(24) Kitchin, J. R.; Nørskov, J. K.; Barteau, M. A.; Chen, J. G. *J. Chem. Phys.* **2004**, *120*, 10240–10246.
(25) Gelatt, C. D.; Ehrenreich, H. *Phys. Rev. B* **1974**, *10*, 398.
(26) Kitchin, J. R.; Nørskov, J. K.; Barteau, M. A.; Chen, J. G. *Phys. Rev. Lett.* **2004**, *93*, 156801.
(27) Zhang, J.; Vukmirovic, M. B.; Xu, Y.; Mavrikakis, M.; Adzic, R. R. *Angew. Chem., Int. Ed.* **2005**, *44*, 2132–2135.
(28) Ghosh, T.; Vukmirovic, M. B.; DiSalvo, F. J.; Adzic, R. R. *J. Am. Chem. Soc.* **2010**, *132*, 906–907.
(29) Stamenković, V.; Mun, B. S.; Mayrhofer, K. J. J.; Ross, P. N.; Marković, N. M.; Rossmeisl, J.; Greeley, J.; Nørskov, J. K. *Angew. Chem., Int. Ed.* **2006**, *45*, 2897–2901.
(30) Stamenković, V. R.; Mun, B. S.; Mayrhofer, K. J. J.; Ross, P. N.; Marković, N. M. *J. Am. Chem. Soc.* **2006**, *128*, 8813–8819.
(31) Gong, K.; Su, D.; Adzic, R. R. *J. Am. Chem. Soc.* **2010**, *132*, 14364–14366.
(32) Xing, Y.; Cai, Y.; Vukmirovic, M. B.; Zhou, W.; Karan, H.; Wang, J. X.; Adzic, R. R. *J. Phys. Chem. Lett.* **2010**, *1*, 3238–3242.
(33) Mizutani, U. *Hume-Rothery Rules for Structurally Complex Alloy Phases*; CRC Press: Boca Raton, FL, 2010.